Evaluation of the diagenetic role of iron as a sulfide buffer at Cape Lookout Bight, North Carolina (USA)

Bo He

A thesis submitted to the faculty of the University of North Carolina at Chapel Hill in partial fulfillment of the requirements for the degree Master of Sciences in the Department of Geological Sciences

Chapel Hill
2009

Approved by:
Advidor: Dr. Stephen Meyers
Reader: Dr. Marc Alperin
Reader: Dr. Larry Benninger
Reader: Dr. Donna Surge

© 2009
Bo He
ALL RIGHTS RESERVED

ABSTRACT

Bo He: Evaluation of the diagenetic role of iron as a sulfide buffer at Cape Lookout Bight, North Carolina (USA)
(Under the direction of Stephen Meyers and Marc Alperin)

Organic matter accumulation in marine environments is influenced by a range of factors, including primary production and the degree of subsequent biochemical degradation. Iron availability has important impacts on primary production rate and thus it has been argued that an increase in iron supply to the oceans could result in enhanced primary production and organic matter burial. This study investigates an alternative hypothesis, designated the "Sulfide Buffer/Phosphorous Trap Hypothesis", through a series of "iron addition" macrocosm experiments with modern sediments collected from Cape Lookout Bight (North Carolina). Results of the incubation experiments are used to evaluate the hypothesis that an increase in iron delivery to the sediments can buffer the accumulation of hydrogen sulfide within pore water, enhance the oxygen penetration depth and degree of bioturbation/bioirrigation, and increase the remineralization of organic matter. This biogeochemical hypothesis provides a mechanism that could link iron concentration and organic matter burial in ancient marine environments.

ACKNOWLEDGEMENTS

I wish to express my deepest gratitude to my advisor, Dr. Stephen Meyers, for creating this project and supporting me during my master's study at Chapel Hill. His guidance and generosity made this study possible. I would also like to thank Dr. Marc Alperin, of the Department of Marine Sciences, whose constant encouragement is greatly appreciated. The advice and help of the other members from my thesis committee, Dr. Larry Benninger and Dr. Donna Surge, were invaluable. Thanks to Dr. Jonathan Lees and Dr. Zhengyuan Zhu at the Department of Statistics and Operations Research for instructing and inspiring me on the statistical approaches. Many thanks to graduate student colleagues of mine, Wesley Ingram, Dylan Malynn, and Ting Wang, for their valuable suggestion and discussion.

I would like to thank my ever-loving and dearest parents for their endless support and encouragement. Lastly I would like to thank my girlfriend Nanxi Bian for loving and supporting me and whose understanding and comfort helped me through difficult times.

The Martin fund provided financial support for the summers of 2008 and 2009. The Department of Geological Sciences made this project possible with support during various semesters.

TABLE OF CONTENTS

LIST OF TABLES

LIST OF FIGURES

LIST OF ABBREVIATIONS AND SYMBOLS

CH_2O	Organic matter
SRZ	Sulfate reduction zone
OM	Organic matter
MAR	Mass accumulation rate
CLB	Cape Lookout Bight
DBL	Diffusive boundary layer
SWI	Sediment-water interface
OPD	Oxygen penetration depth
XRF	X-ray fluorescence
ERD	Efficient redistribution depth
LSE	Least square estimate
RSS	Residual sum of squares
BLUE	Best Linear Unbiased Estimate
LUE	Linear Unbiased Estimate
i.i.d.	Independent and identically distributed
OLS	Ordinary least square
1-α	Confidence level
C.I.	Confidence interval
LAD	Least absolute deviation
OAE	Oceanic Anoxic Event

Introduction

Past studies suggest that iron delivery to the ocean can serve as an important control on primary production rate (Martin, 1990), and potentially on organic matter burial rate (e.g., Leckie et al., 2002). Iron is an important micronutrient for living systems, particularly in the photosynthetic process. Mesoscale iron enrichment experiments (Martin et al., 1994; Coale et al., 1996) conducted in the high nutrient low chlorophyll regions of the ocean have demonstrated a relationship between the addition of iron and an increase of primary production. In this study we will test an alternative hypothesis regarding to the role of iron in driving marine biogeochemistry and organic matter burial: that an enhancement of iron delivery to marine sediments could result in decreased organic matter burial rate through biogeochemical linkages that impact early diagenetic organic matter remineralization. This hypothesis is designated the "Sulfide Buffer/Phosphorous Trap Hypothesis" (Meyers, 2007).

Background

The production, remineralization, and burial of organic matter are essential controls on atmospheric carbon dioxide and oxygen levels (Arthur et al., 1985; Berner and Canfield, 1989) throughout geologic time, and have also been linked to the evolution of metazoans. The fate of organic matter is also important for studying global climate

change (Arthur et al., 1988), as well as for understanding petroleum generation. For these reasons, much research has focused on evaluating the fundamental controls on organic matter production, preservation and burial (Demaison and Moore, 1980; Ibach et al., 1982; Pedersen and Calvert, 1990; Hedges and Keil, 1995; and many others).

The principle source of organic matter that accumulates in the marine sedimentary environment is phytoplankton (Demaison and Moore, 1980), composed mainly of single-cell algae living in the euphotic zone, the uppermost layer of the water column where light can penetrate and support photosynthesis. Limiting factors for primary production besides light include the availability of nutrients, such as carbon dioxide, nitrate, phosphate, and iron. Another source of photosynthetically-derived organic matter to the marine environment is via terrestrial input, transported by rivers and streams, largely dependent on the amount of rainfall on landmasses (Demaison and Moore, 1980).

After it is produced, organic matter is inherently thermodynamically unstable and will transform into a more stable state by serving as the energy source for living organisms. Bacterial degradation proceeds quickly and efficiently in oxic water. The overall degradation process by aerobic bacteria can be illustrated as:

$$CH_2O + O_2 \rightarrow CO_2 + H_2O.$$

When oxygen supply in the water is exhausted, organic matter degradation will continue by dysaerobic bacteria using MnO_2, nitrate and iron oxides almost simultaneously as the oxidants (or, electron acceptors, a more general term) by the simplified reactions (Froelich et al., 1979):

$$CH_2O + 2MnO_2 + 4H^+ \rightarrow CO_2 + 2Mn^{2+} + 3H_2O;$$

$$5CH_2O + 4NO_3^- + 4H^+ \rightarrow 5CO_2 + 7H_2O + 2N_2;$$

$$CH_2O + 2Fe_2O_3 + 8H^+ \rightarrow CO_2 + 4Fe^{2+} + 5H_2O.$$

After MnO_2, nitrate and iron oxide is consumed, the remineralization of organic matter will continue by the anaerobic process of sulfate reduction, which can be generalized as:

$$2CH_2O + SO_4^{2-} + 2H^+ \rightarrow 2CO_2 + 2H_2O + H_2S.$$

The least efficient and final step in anaerobic metabolism is methanogenesis; since a great deal of CO_2 is accumulated due to previous processes, CO_2 and organic acids are employed as oxidants for the final step.

Of central importance to the present study, a byproduct of organic matter degradation by sulfate reduction is hydrogen sulfide (H_2S), which is toxic to living aerobic organisms in the water column and sediments. Furthermore, the anaerobic degradation that occurs in H_2S–rich environments is less efficient than aerobic decomposition (Demaison and Moore, 1980). For instance, in the Black Sea, one of the most representative euxinic and anoxic environment for organic matter preservation, about 80% of the original organic matter input is degraded within the top 200 meters of oxic water. The remaining 20% escapes into the anoxic, hydrogen sulfide enriched lower water column, where half of the organic material (10%) is further decomposed and recycled by anaerobic bacteria. Finally, about 5% of the original organic matter is solubilized in the anoxic water and 5% accumulates in the sediments (Demaison and Moore, 1980; Deuser, 1971). In contrast, under typical aerobic environment and open oceans, less than 0.5% of the organic matter

originally produced in the surface layer is buried and preserved (Demaison and Moore, 1980).

A number of factors other than primary production rate and oxygen availability can also impact the accumulation of organic matter, such as the sediment particle size and sedimentation rate (Ibach et al., 1982; Hedges and Keil, 1995). However, the two most common models for organic matter burial invoke either the development of stratified euxinic environments (Demaison and Moore, 1980) or changes in the primary production rate (Pedersen and Calvert, 1990). The hypothesis investigated in this study, termed the "Sulfide Buffer/Phosphorous Trap Hypothesis", however, does not require either of these prerequisites.

The Sulfide Buffer/Phosphorous Trap Hypothesis

Figure 1 (from Meyers, 2007) intuitively illustrates how changes in iron input could affect and adjust the level of hydrogen sulfide in the sediments, the oxygen exposure time of organic matter and the degree of organic matter remineralization, assuming a constant organic matter input flux. In this conceptual model, Stage B (Figure 1B) is characterized by a decreased iron input, compared with an initial Stable Stage A (Figure 1A). The decrease of reactive iron input enables H_2S to accumulate in the uppermost region of the sulfate reduction zone (since less is removed by reaction with iron) and enhances H_2S diffusion into the overlying bioturbation zone. In response to the elevated H_2S concentration, the depth of bioturbation/biodiffusion decreases, and the upper interface of the sulfate reduction zone (SRZ) shoals. Oxygen exposure time decreases due to the shoaling of the SRZ, allowing more labile organic matter to enter the SRZ and further

enhancing the production of H_2S, yielding a positive feedback. Equally important, because the iron oxyhydroxide phases that are highly reactive in sulfidization are also highly efficient in scavenging phosphorous (Ruttenberg, 2003), a decrease in reactive iron delivery can enhance the phosphorous return flux into the water column to support photosynthesis. The net consequence of these biogeochemical interactions is a positive feedback that will accelerate shoaling the SRZ until it reaches another potential end member, such as the sediment-water interface (Stable Stage 2; Figure 1C).

It has been previously demonstrated (Meyers, 2007) that in most modern marine environments, relatively modest quantities of iron could be sufficient to buffer the hydrogen sulfide accumulation, and that the kinetics of iron sulfidization is also rapid enough to remove sulfide as quickly as it is produced. Moreover, the concentration of iron within sediments throughout geological history is variable enough for iron to function as a primary control on organic matter burial, and may also have implications for Oceanic Anoxic Events (Meyers, 2007).

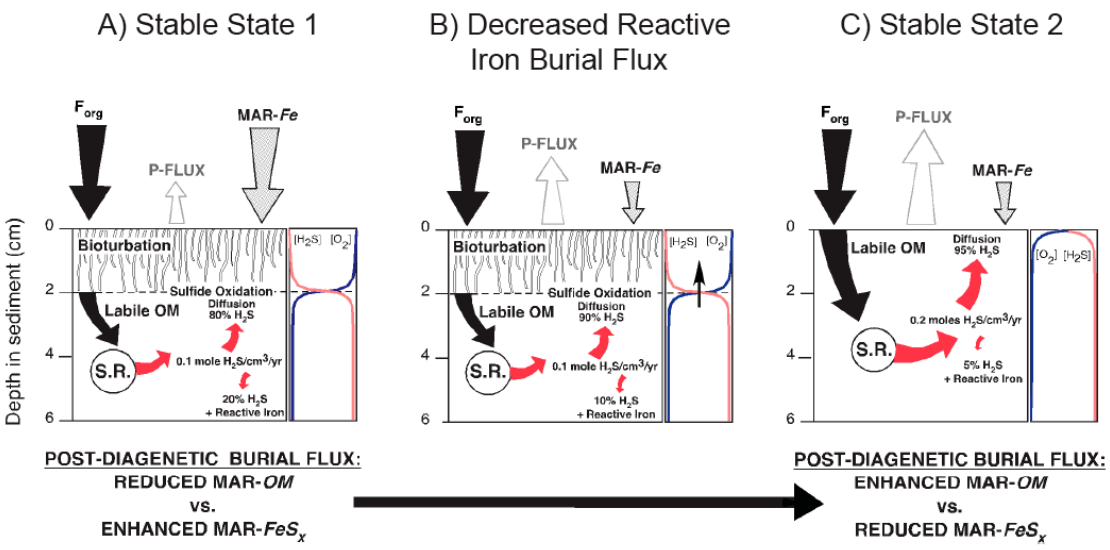

Figure 1. Proposed linkage between iron burial, hydrogen sulfide concentration, oxygen penetration depth, dissolved phosphorus flux and organic matter burial (the "Sulfide Buffer/Phosphorous Trap Hypothesis"). Arrow sizes reflect the magnitudes of the fluxes. OM = organic matter, SR = sulfate reduction, MAR = mass accumulation rate. All fluxes are purely illustrative, intended to convey the basic premise of the hypothesis. (Figure and caption, from Meyers, 2007)

This Study

This study develops a new experimental protocol for assessing organic matter burial and testing the role of iron as a sulfide buffer during early diagenesis by conducting a series of "iron addition" incubation experiments with modern sediments from Cape Lookout Bight (CLB, North Carolina, Figure 2). Cape Lookout Bight is a shallow coastal marine environment (< 8m) with an oxygenated water column, but organic-carbon rich

sediments dominated by sulfate reduction and methanogenesis. The specific hypotheses involved in the experiments are:

Hypothesis 1: A modest increase in reactive iron concentration will buffer the hydrogen sulfide (H_2S) accumulation in sediments from Cape Lookout Bight.

Hypothesis 2: Increased buffering of H_2S will increase the oxygen penetration depth and allow for higher degree of bioturbation/bioirrigation.

This study includes one coring campaign and 5 "iron addition" incubation experiments. One site was chosen for sediment collection (A-1 in Figure 2). Our study introduces a new experimental methodology that involves using both oxygen microelectrode measurements and X-ray fluorescence scanning (details will be discussed in the Methodology section). Table 1 illustrates the basic procedure of these experiments. This study will specifically focus on the diagenetic role of iron as a buffer for pore water sulfide, and its impacts on oxygen penetration and bioturbation/bioirrigation.

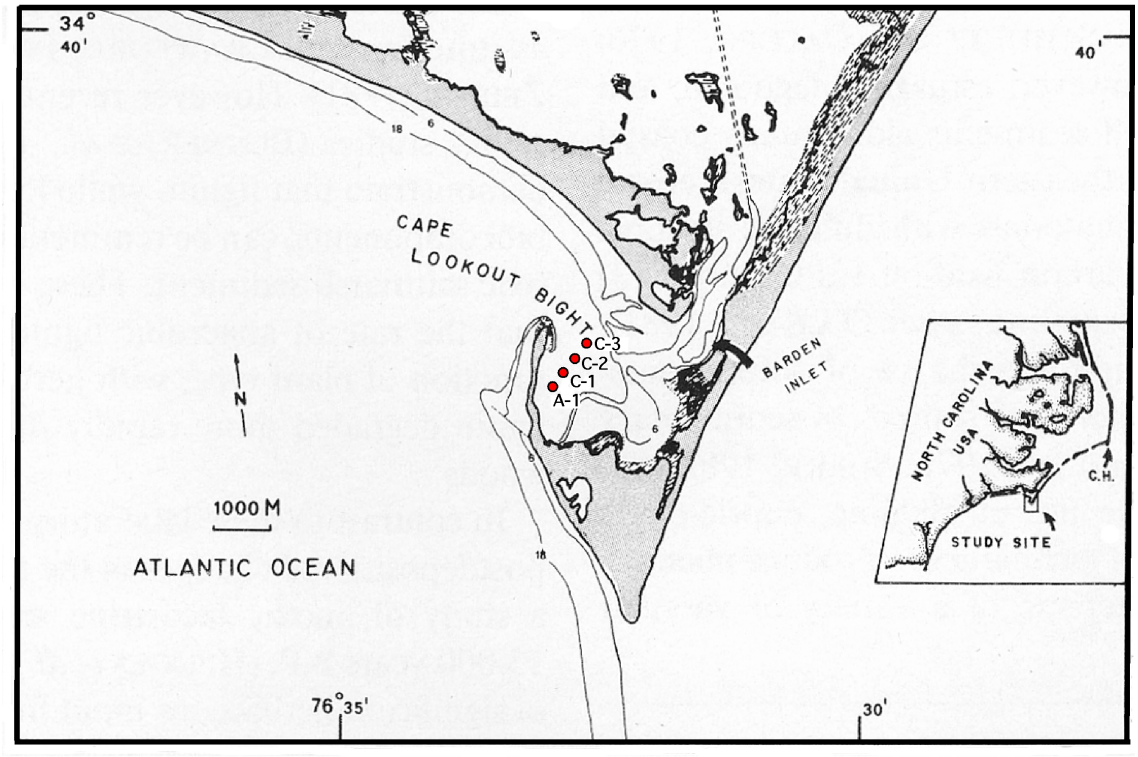

Figure 2. Map of the study area, Cape Lookout Bight (Outer Banks, North Carolina) with field sites A-1, C-1, C-2 and C-3 identified (Modified after Haddad and Martens, 1987 and Bartlett, 1981).

Methodology

Core collection

50 cm depth side-by-side diver-taken cores, as well as the overlying water, were collected from site A-1 on April 30th, 2008 (5 cores, Figure 2). Core tops, together with 2 cm of overlying water, were covered by rubber caps and kept at ambient temperature (est. 30 °C) during transportation to the core lab at UNC. The inclusion of 2 cm of overlying

water helped to keep the integrity of the surficial sediment layer during transport, and an air hole in the caps sustained oxygen supply into the water and prevented anoxia from developing.

Synthetic sediment preparation

10 wt% of samarium oxide (Sm_2O_3) was added to clay (bentonite) as a tracer element to assess bioturbation. To adsorb the samarium onto the clay particles, first, an excess of hydrochloric acid (1N HCl) was used to dissolve the samarium oxide, followed by the addition of sodium hydroxide (1N NaOH) to neutralize the solution, while carefully monitoring pH. Various amounts (3-6 elemental weight percent out of total sediment mass) of ferric iron (in the form of hematite powder, Fe_2O_3) were then added to the synthetic sediments. After thorough mixing, the sediments were rinsed and centrifuged three times with Milli-Q water to remove extra sodium chloride (NaCl) produced during acid neutralization. Then the sediments were dried in the oven at 50 °C for 48 hours, crushed into fine powder, and mixed with seawater collected from Cape Lookout Bight.

Treatments

The five sediment cores were subjected to five different treatments. Two cores were chosen as controls: one (core 1) with no addition, and the other (core 2) with an addition of clay and Sm. Three other cores were prepared with clay, Sm and extra iron addition. The synthetic sediments were added on top of the cores as an additional sediment layer

(approximate thickness: 0.5 cm) after removing the seawater from the macrocosm chamber down to the sediment-water interface. After synthetic sediment addition, seawater from CLB was carefully added back to the macrocosm chamber. The overlying water was kept oxygenated by bubbling air into the water throughout the experiments. After the macrocosm experiments were initiated, sediment cores were left in the laboratory at ambient temperature (est. 23 °C) to attain equilibrium for one week, covered by a thick lid that prevented light penetration. The overlying seawater was renewed every week (after OPD measurements; see below) to avoid the build up of organic matter remineralization products.

Assessment

The impact of iron concentration on oxygen penetration depth and bioturbation/bioirrigation is assessed using (1) oxygen microelectrode measurements and (2) X-ray fluorescence scanning of subcores. The oxygen microelectrode employed in this study has a 100-micron diameter tip and was calibrated in oxygen-saturated seawater before measurements. The microelectrode was mounted onto a micromanipulator and lowered into the sediments to measure in-situ pore water oxygen concentration. The depth interval step size of the microelectrode measurements varied from a few microns to a few millimeters depending on the oxygen gradient, with a goal of defining the detailed shape of the oxygen profile. We targeted possible burrows and other interesting features (e.g., organic matter piles), as well as "background" values from non-burrowed surface area.

The incubation experiments lasted for three months, including four rounds of OPD measurements (measurement dates are reported in the following text). Each round of OPD measurements took five days on average to complete. After the fourth round of OPD measurements was complete, the overlying seawater was removed and the cores were cooled in the refrigerator at 10 °C for 8 hours before they were subcored and scanned. X-ray fluorescence scanning evaluated the vertical redistribution of samarium to estimate bioturbation. The sediment subcores were attached onto a flat measuring panel, which allowed lateral movement to evaluate multiple vertical transects. The scanning data was acquired at one millimeter resolution (along core), and replicate scans were performed at one centimeter resolution. XRF analyses utilized a 10 kv/1000 uA XRF source setting, with an XRF detector count time of 90 seconds per measurement.

Calibration

The voltage measurements from the microelectrode are calibrated to oxygen concentration using two end points: (1) oxygen-saturated seawater at known temperature, and (2) anoxic pore water at depth in the incubation experiments (the depth in the sediments where voltage plateaus and does not further change is assumed to have zero oxygen concentration). For the X-ray fluorescence analysis, the samarium tracer scan results are XRF counts that represent relative samarium concentration within the sediments. Calibration was performed as follows to convert XRF counts into Sm concentration. A series of clay-based synthetic sediment samples, with identical concentration of iron (3 wt%) but different percentage of samarium addition (1-9 wt%), were analyzed to develop a calibration equation for Sm concentration. The results are

plotted in Figure 3 and a linear relationship is exhibited between XRF counts and samarium weight percentage. This equation is used to calibrate Sm concentration (wt%) in the sediments, given the instrumental XRF counts.

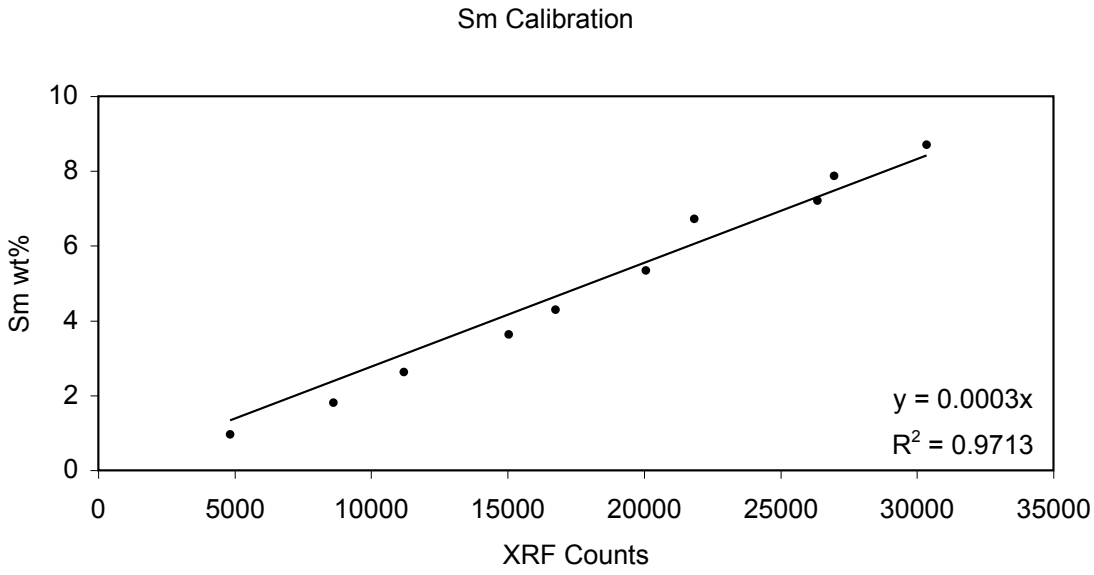

Figure 3. Scan results for synthetic sediment samples with known composition, exhibited strong (high R^2 value, forced through origin) and positive linear correlation between instrumental X-ray fluorescence counts and in-situ Sm concentrations (wt%).

Statistical Analysis Background

In any scientific problem, two aspects of statistical analysis are commonly employed after data collection is finished: (1) initial data analysis (or, descriptive statistics) and (2) inferential statistics. Descriptive statistics includes graphical display of the data, summarizing and organizing data; while inferential statistics focuses on reaching

conclusions and making decisions via, for example, linear regression analysis as well as hypothesis testing. Regression analysis proposes a model to explain the relationship between a single variable Y (response, output, or dependent variable) and other variables $X_1, X_2, \ldots X_p$ (predictor, input or independent variable); more importantly, the models can be used to explain effects of the predictor variables, describe data structure, or be used for prediction. It is important to note that the underlying "truth", which could be simplified as: $y_{n\times 1} = X_{n\times(p+1)}\beta_{(p+1)\times 1} + \varepsilon_{n\times 1}$, remains impossible to estimate directly, given a finite number of observations (in the equation listed above, $X_{n\times(p+1)}$ is the design matrix, β is the coefficient and $\varepsilon_{n\times 1}$ represents the error term). In our study, the response variable is *oxygen penetration depth* (OPD) and the predictors include elapsed *time*, *addition of iron*, and *number of burrows* and so on (details discussed in the following text).

To estimate β, $\hat{\beta}$ could be calculated by several criteria. The least square estimate (LSE) is one of the most commonly used criteria and has been widely applied in science, pharmacy, finance, sociology, and other fields. The goal of LSE is to minimize the square error: $\min_{\beta} \sum_{i=1}^{n} \varepsilon_i^2 = \varepsilon^T \varepsilon = (y - X\beta)^T (y - X\beta)$; and the goodness of fit is usually assessed by the residual sum of squares (RSS): $\sum_i (y_i - \hat{y}_i)^2$ and R^2 value (a value between 0 and 1): $R^2 = 1 - \frac{\sum_i (y_i - \hat{y}_i)^2}{\sum_i (y_i - \bar{y})^2} = \frac{\sum_i (\hat{y}_i - \bar{y})^2}{\sum_i (y_i - \bar{y})^2}$. An R^2 value close to 1 usually indicates good fit but is not always true because a wrong model might also yield high R^2; on the contrary, a low R^2 value doesn't necessarily mean there is no relationship between response and predictors because it could be caused by a slight trend with high variance. As a result,

regression diagnostics have to be performed to determine the assumptions and fit of the model, such as checking unusual observations, multi-collinearity, normality, and error assumptions.

It has also been proven by the Gauss-Markov Theorem that least square estimation is the Best Linear Unbiased Estimate (BLUE) among all the linear unbiased estimates (LUE), assuming a full rank design matrix and constant error. However, this standard assumption about the error term is sometimes violated since it is not always independent and identically distributed (i.i.d.), in which case other types of regression should be used instead.

Transformation of the response and/or predictors can improve the fit of the model and correct for violation of model assumptions. Often times, we have more options in choosing the transformations on the predictors than on the response. The Box-Cox method is one of the most popular ways to determine a transformation on the response. It is specially designed for strictly positive dependent variables and allows some flexibility in choosing the transformation to identify the best fit of the data. The Box-Cox method transforms the response: $y \to g_\lambda(y)$ where the family transformation index by λ is:

$$g_\lambda(y) = \begin{cases} \dfrac{y^\lambda - 1}{\lambda}, \lambda \neq 0 \\ \log y, \lambda = 0 \end{cases}.$$

The goal of this method is to choose an interpretable λ to maximize the likelihood profile, which is calculated as shown below assuming normality of error:

$$L(\lambda) = -\frac{1}{2}\log(RSS_\lambda / n) + (\lambda - 1)\sum \log y_i .$$

Transformation of the independent variables also provides improvements as well as more flexibility. Commonly used predictor transformations include Broken Stick Regression, polynomials, and regression splines, and so on. It usually takes experimentation to determine the appropriate transformation, and the transformed model should always be interpretable. In addition, not all the transformations are necessary and one should balance the goodness of fit and the models interpretability.

Results and Discussion

We collected four sets of OPD measurements (211 measurements in total) over a three-month period, and each individual set contains 10-14 oxygen profiles for each of the five cores. The profiles delineate changes in oxygen concentration from the well-oxygenated water overlying the sediments, to the anoxic sediment pore water at depth (Figure 4). The blue profile in Figure 4 displays a typical non-burrowed "background" oxygen profile with different vertical zones. The diffusive boundary layer (DBL), located just above the sediment-water interface (SWI), is the region where oxygen concentration decreases linearly with depth. The SWI occurs at the depth where the oxygen concentration deviates from this linear trend (please refer to Appendix A). In this study, the oxygen depletion depth (ODD) is defined as the depth where oxygen concentration reaches less than 0.5% of the initial saturated oxygen concentration in the water column, while oxygen penetration depth (OPD) is the vertical thickness from the SWI to the ODD.

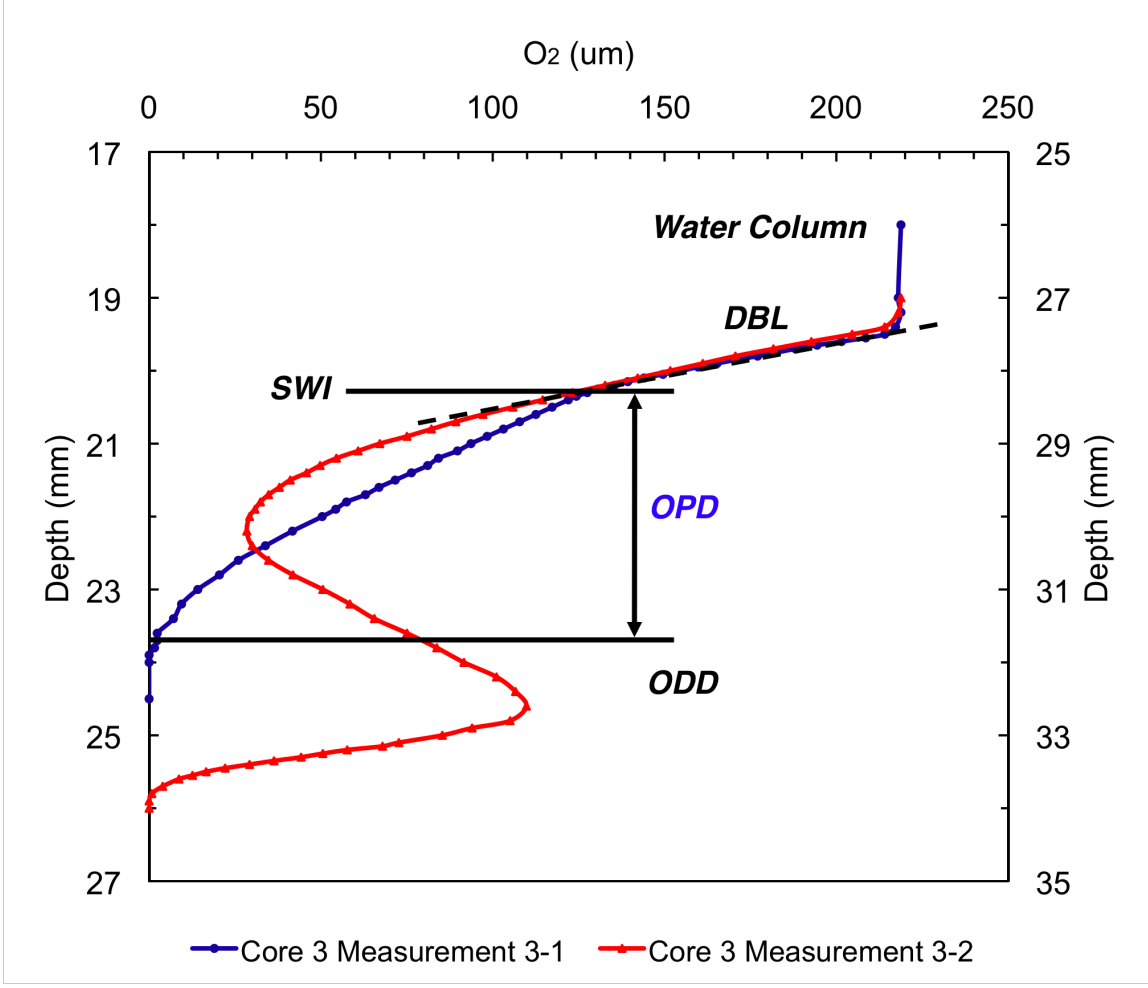

Figure 4. Oxygen profile measurements from the water column into the sediments. Blue profile represents a typical non-burrowed "background" oxygen profile, where different zonations (diffusive boundary layer = DBL, sediment-water interface = SWI, oxygen penetration depth = OPD, and oxygen depletion depth = ODD) can be identified. Red line represents oxygen profile from a burrowing area, where the oxygen penetration depth is greatly influenced by burrowing activities.

Several methods are available to determine OPD (communication with Marc Alperin, refer to Appendix A). For the DBL and OPD calculations presented here, it is

assumed that the sediment surface is homogenous and generally even; however, in reality, this assumption is sometimes violated by biological activities (bioturbation, etc.) (refer to the red profile in Figure 4). This problem can make it difficult to determine the location of the SWI in the oxygen profile, which is critical for the estimation of total OPD. Considering that all the profiles do not share an ideal oxygen depth profile (from water column to DBL to SWI), we have selected 45 profiles with easily identifiable DBL and SWI and calculated the average thickness of the DBL. The average DBL thickness is used to predict OPD by subtracting it from the total depth between top of DBL and ODD ($ODD - DBL_{Top} - DBL_{Ave}$), both of which are easily determined. We believe that 45 profiles (21.3% of the population) are statistically sufficient to represent the total 211 measurements, and the selected 45 oxygen profiles yield an average DBL of 1.21 ± 0.33 mm (with 1 s.d.). The OPD measurements thus calculated yield detailed contour maps of oxygen penetration over time in each core.

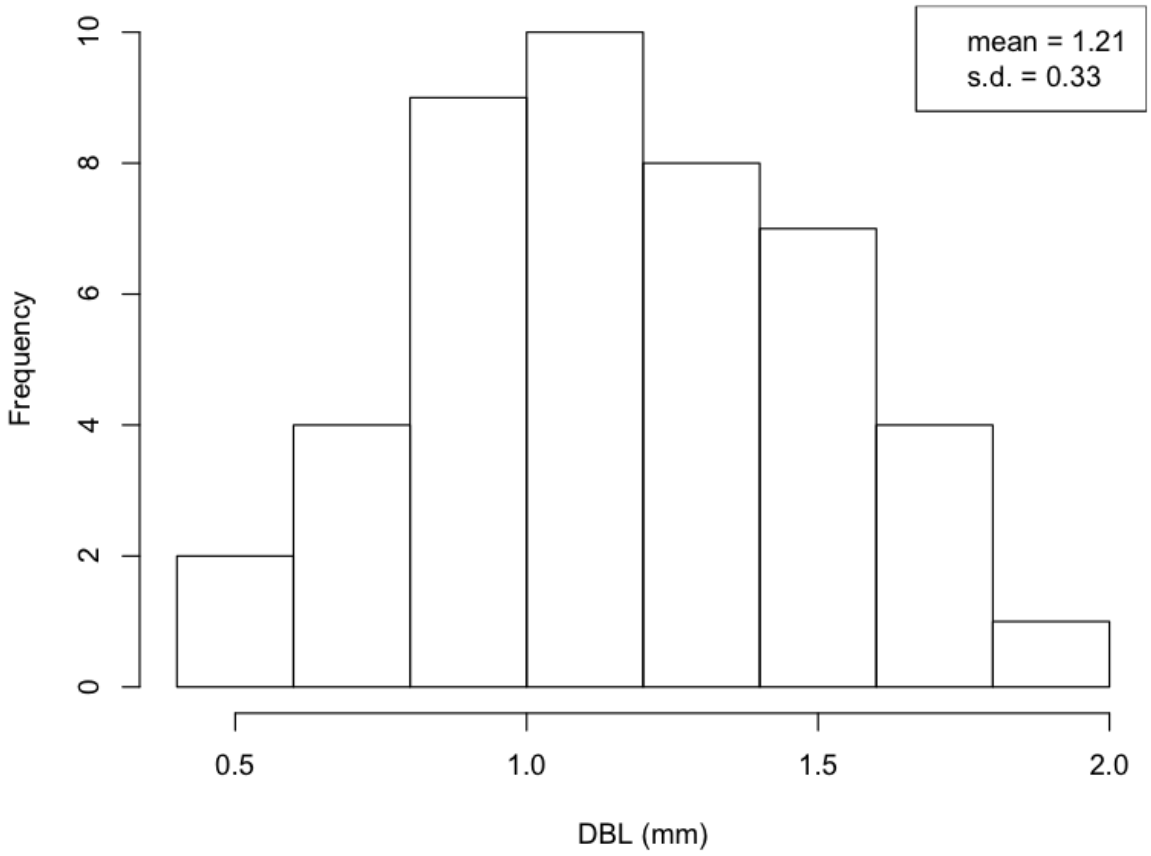

Figure 5. Histogram of DBL thickness determined from the selected 45 oxygen depth profiles. The DBL data, with a mean value of 1.21 mm and standard deviation of 0.33 mm, falls into the range of DBL from various marine environments (1-2 mm, Sarmiento and Gruber, 2005).

Figure 6 displays OPD contour plots for the cores during each of the four measurement periods. Solid circles in the plots identify the position of each oxygen profile measurement, and the color indicates oxygen penetration depth. These contoured surfaces are generated using a minimum curvature spline (GMT, *gmt.soest.hawaii.edu*) interpolation between the measurement points. All plots share the same logarithmic color

scale, where cold colors (blue) represent shallow OPD and warm colors (red) represent deep OPD. Considering all the cores, the overall OPD averages 2.27 mm.

In our discussion below, core 1 (no addition) and core 2 (addition of clay, Sm and no iron addition) represent controls for the OPD measurements. As the experiments proceed (left to right in figure 6), the general pattern of OPD in the control experiments becomes shallower (the colder color area expands), which is consistent with a decrease in bioturbation/bioirrigation through time. In contrast, core 3 (clay, Sm and 3 wt% iron addition) displays a reversed temporal pattern in OPD: (1) during measurement 3, it has the highest OPD (13 mm), compared to the overall average OPD of 2.27 mm; (2) In measurement 4, although certain extreme values disappear, the general pattern suggests deeper oxygen penetration. One possible explanation for the results observed in core 3 is that the added iron has buffered hydrogen sulfide in the pore water, enhancing bioturbation/bioirrigation. As a consequence, more oxygen penetrates into the sediments to fuel aerobic degradation and hydrogen sulfide accumulation.

X-ray fluorescence scanning provides additional information about cores 2 and 3 from another perspective. Figure 7 is a summary of fine-scan (1 mm step size) results from two adjacent vertical transects for each core (blue and red lines). The XRF counts on the top horizontal axis represent qualitative samarium concentration, while the bottom horizontal axis represents the calibrated weight percentage of samarium in the sediments. The Sm effective redistribution depth (ERD), which also represents the depth of bioturbation, is this thickness from the SWI (with highest Sm concentration) to the depth

where it approaches the background noise level. The Sm ERD in control core 2 is close to 6 mm (±1.5), while the Sm ERD in core 3 (with 3 wt% addition of iron) is approaching 12 mm (±0.5). The comparison between core 2 and core 3 is in good agreement with measured oxygen penetration depths; increased OPD is associated with an increase in Sm ERD, which could be explained by the mechanism of the Sulfide Buffer/Phosphorous Trap Hypothesis. More importantly, it also suggests that we can use the OPD as a proxy for bioturbation depth. Furthermore, since aerobic respiration is thermodynamically the most efficient degradation pathway for organic matter, it is reasonable to assume that OPD should exert a control on organic matter burial rate (Hartnett et. al, 1998).

In contrast to core 3, the results from core 4 (clay, Sm and 4.5 wt% iron addition) and core 5 (clay, Sm and 6 wt% iron addition), do not show any temporal increase in OPD (Figure 6). Instead, these two cores share a similar trend as core 1 and core 2, and the OPD decreases through time. The Sm ERD for core 4 and 5 averages 5.5 mm (±2) and 4 mm (±2.5), respectively. OPD measurements and the Sm ERD are in good agreement and also confirm that this methodology, indeed, can detect bioturbation/bioirrigation from two different perspectives. However, the results from core 4 and core 5 indicate that the variance in OPD cannot be explained solely by various iron treatments, and that other variables also need to be taken into consideration.

In this regard, since the Sulfide Buffer/Phosphorous Trap Hypothesis relies on iron buffering sulfide to enhance bioturbation/ bioirrigation, the number and type of aerobic metazoa (e.g., worms) in the sediments becomes very essential to our discussion. In our

study, we have not quantified the number and type of organisms directly. However, we did observe that core 2 and core 3 had the largest number of burrows and actively digging macrofauna. Additionally, the number and distribution of burrows in these two cores may be "saturated" (maximized) for the core size (10 cm diameter) in this study. Thus, it is very likely that these two cores have fairly adequate and almost equal amount of metazoa. In contrast, core 4 and core 5 didn't have as many burrows or worms and they seemed to have less disturbed surface sediments from the start of the experiments. As a consequence, even though all the cores were collected from exactly the same geographic location, different number of metazoa could explain the observation that core 4 and core 5 do not show a temporally increasing pattern of OPD, or elevated Sm ERD, as was the case in core 3. On the contrary, core 4 and core 5 do have deeper OPD than core 1 at the end of the OPD experiment, which could be due to the role of iron addition as a buffer for sulfide. It is also reasonable to speculate that different types of metazoa could also lead to different OPD and Sm ERD. Multiple factors that could influence OPD and Sm ERD are further investigated below using statistical approaches to evaluate the data.

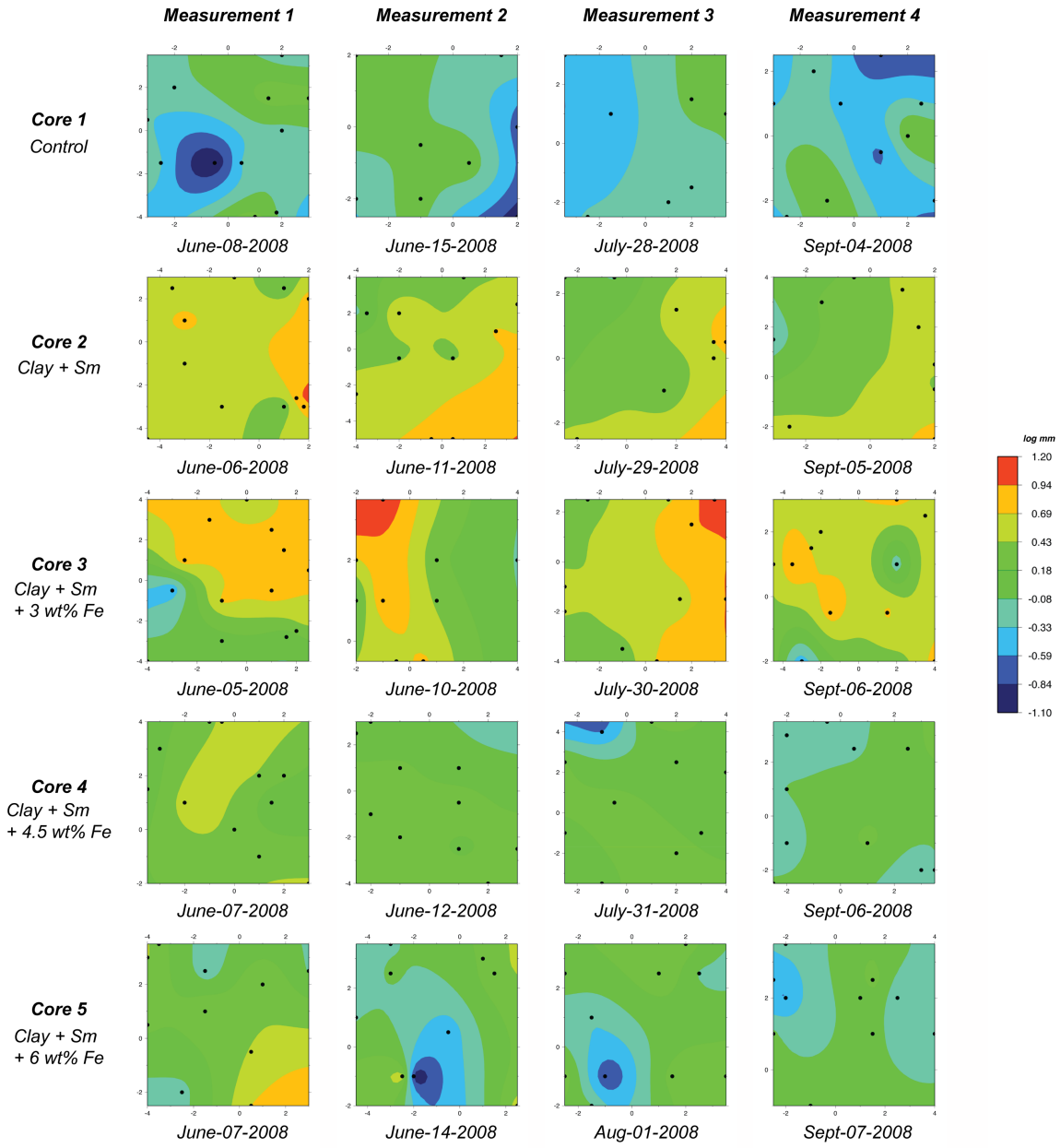

Figure 6. OPD contour map summary, with core information to the left and date of measurement at the bottom of each column. Dark solid circles represent OPD measurements; the coordinates display spatial distribution of OPD measurements, where the origin is the center of the sediment cores. Color scheme to the right indicates OPD: warm colors represent deeper OPDs and cold colors represent shallower OPDs, respectively.

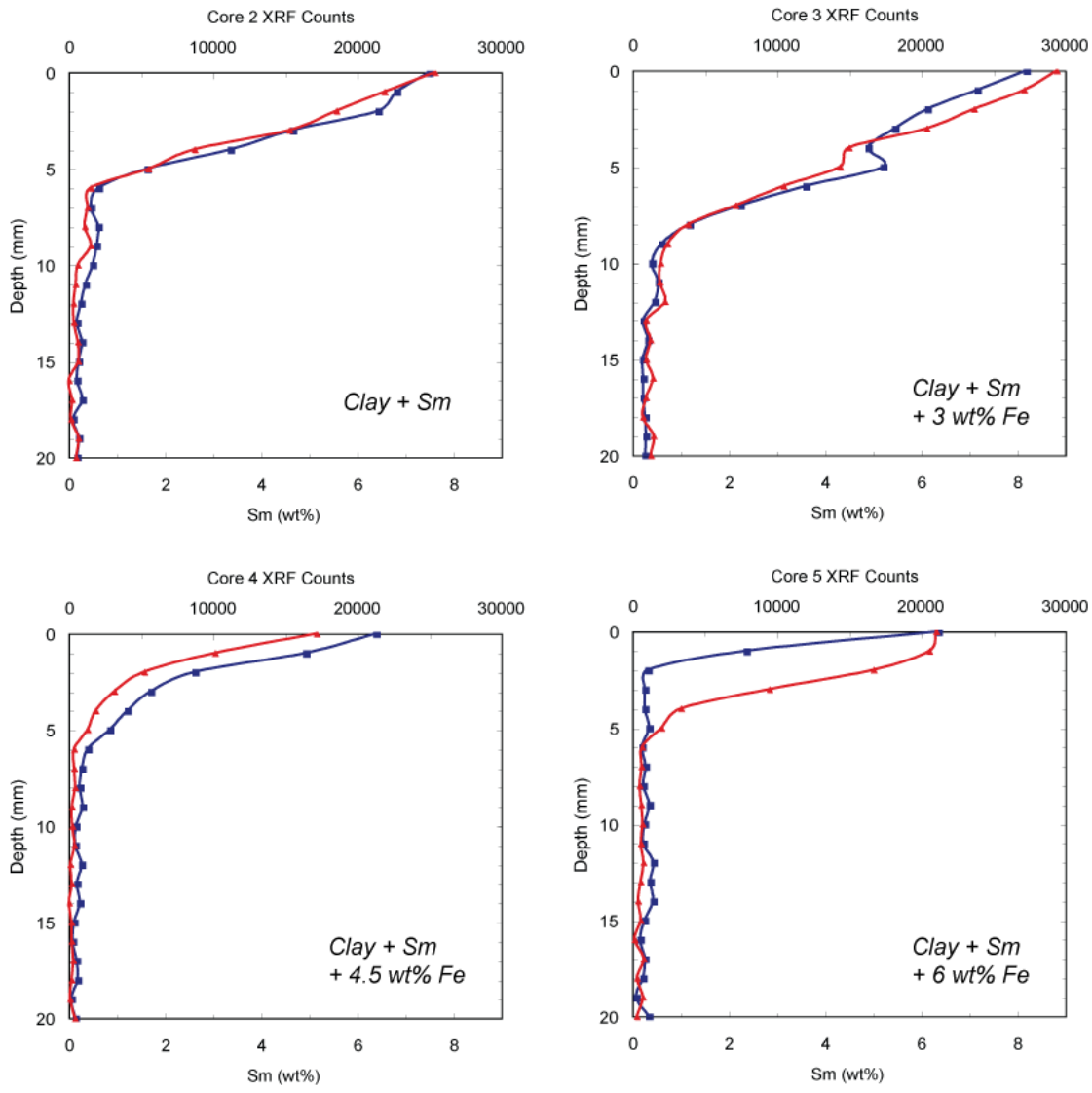

Figure 7. X-ray fluorescence scan results from core 2-4. In each plot, blue and red lines represent adjacent vertical transects. The XRF counts on top axis represent relative samarium concentration, while the bottom axis represents the calibrated weight percentage of samarium within the sediments. Count time was 90 seconds per measurement; voltage and current were set to 10 kv and 1000 uA, respectively.

Statistical Analysis

Initial Data Analysis

In this regression study we fit a statistical model to predict *oxygen penetration depth (OPD, millimeters)*, the response (or, dependent variable). Potential predictors (or, independent variables) include *time (days)*, *number of burrows*, *burrow/nonburrow (0/1)*, and *iron addition (weight percentage)*. Figure 8 displays a scatter plot of all possible data pair-correlations in a variance-covariance fashion.

Statistical Regression Approaches

Several regression methods have been applied to fit models to our data, and the results are listed in Table 2. Ordinary least square (OLS) regression is the most common model and the assumption for OLS is that the data has an independent and identically distributed (i.i.d.) random error term. Estimates and standard errors of the coefficients are listed in the first two columns, followed by calculated statistics and p-values. The null hypothesis and the alternative hypothesis are set as:

$\boldsymbol{H_0}$: the coefficient of the variable is equal to 0, or, the variable is insignificant;

$\boldsymbol{H_1}$: the coefficient of the variable is not equal to 0, or, the variable is significant;

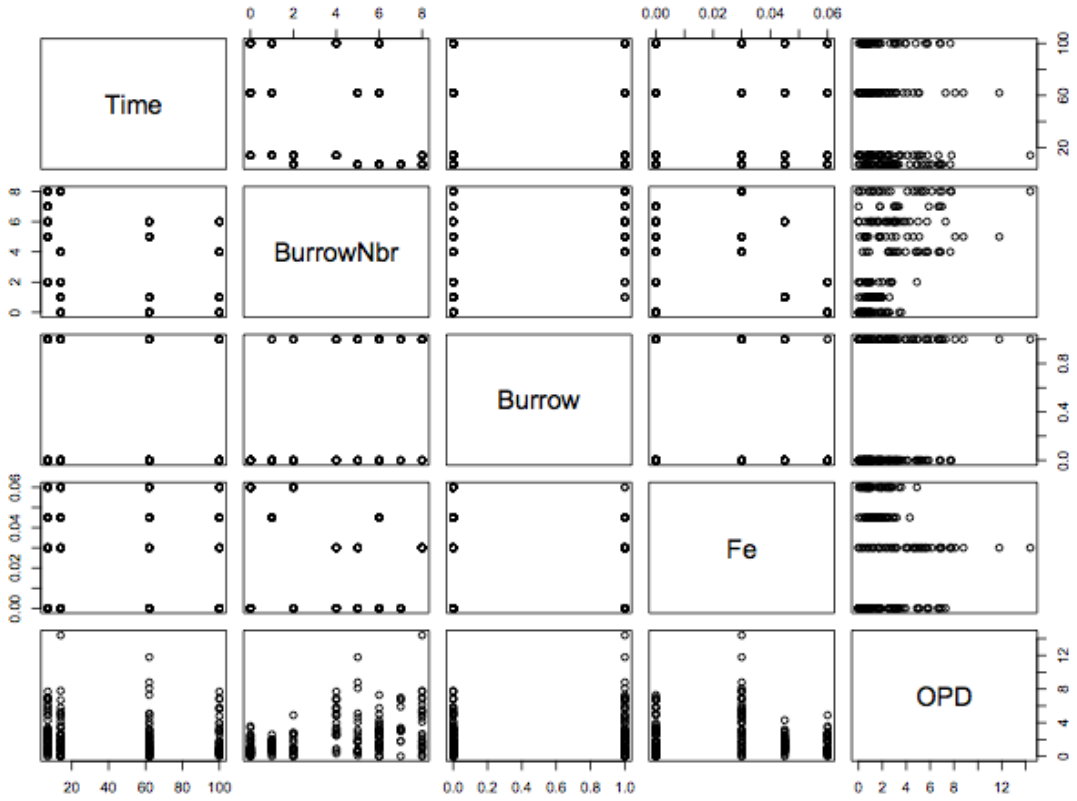

Figure 8. Scatter plots of all data. Circles represent measurements and all the variables are listed along the diagonal of the matrix.

A t-test (or, Students t-test) is performed to calculate the t-statistic and the p-value (Table 2). The p-value yields the probability of attaining the observed measurement (or a more extreme value), given that the null hypothesis is true, and it is compared with α (type I error, which represents the error of rejecting the null hypothesis given that it is true). The α values set for these statistical tests are usually different from case to case, depending on how "risky" the analyst is willing to be when rejecting the null hypothesis. In cases where p-value < α, it indicates that at the confidence level of 1-α, it is statistically reliable to reject the null hypothesis. On the other hand, when p-value > α,

statisticians either choose to perform another test or accept the null hypothesis that the particular variable is statistically insignificant.

In our OLS model (OLS-1), four variables (*time, number of burrow, burrow/nonburrow, iron addition*) serve as potential predictors and α (the type I error) is set to be 0.05. The results from OLS suggest that: (1) the dependent variable (OPD) is positively correlated with all the four independent variables; (2) at 95% confidence level, we can reject the null hypothesis that variables "*number of the burrows"* and "*iron addition"* are not significant, and thus infer that these two variables are related to the variance in OPD; (3) if we were willing to raise the tolerance of α (the type I error), we could also accept that "*time"* is a significant variable in our model, however, "*burrow/nonburrow"* is apparently insignificant, and thus it can be eliminated from the improved least square model (OLS-2).

However, the total r-square value (0.2453) from the OLS model (OLS-2) is fairly low, which, as mentioned earlier, could be caused by a slight trend with high variance or violation of the model assumption (i.i.d. error). The residuals from the model are plotted against fitted values, and the plot (Figure 9) displays a special and unique structure known as heteroscedasticity, which indicates non-constant residual variance. In addition, we know that the model only has a slight (not steep) trend (low regression coeffieients) and relatively high variance, so the low r-square value is mostly likely caused by both non-constant variance (violation of OLS assumption) and high variance (data scattering).

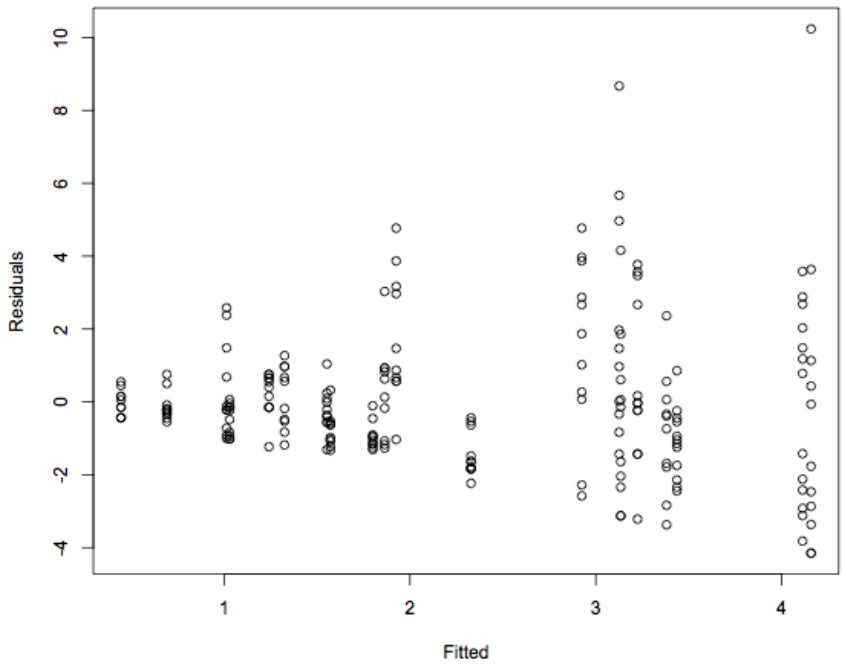

Figure 9. Residuals plotted against fitted value for ordinary least square model (OLS-2).

Different procedures can be taken to improve the fit of the model and to determine the best transformation of the output (e.g., the Box-Cox method) and the input (e.g., polynomials). The lambda value from the Box-Cox method is selected to maximize the likelihood profile (Figure 10), as discussed earlier in the text. Analysis of the OPD data indicates an optimal lambda of 0.35, and thus, it is reasonable to choose 0.3 (the cubic root) as the most appropriate transformation for the output for the sake of interpretability.

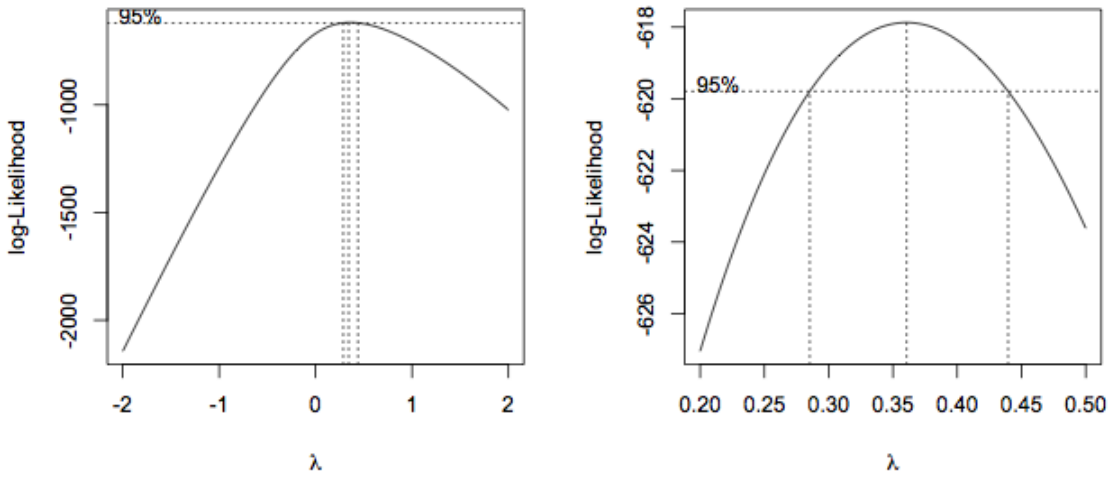

Figure 10. Box-Cox transformation of the dependent variable (OPD). The right panel is a zoom in of the left panel, both of which indicate an optimal lambda, 0.36, to maximize the likelihood profile.

This transformed model (OLS-3), however, still does not have a satisfying r-square value (0.2324). We also tried to refit a model (OLS-4) with a transformation on both the dependent variable (Box-Cox method) and the independent variables (polynomials, the order of 3), but the r-square value still isn't substantially higher (0.2866). However, although the r-square value is not improved, both of the regression models indicate that "*number of burrows"* and "*iron addition"* are two significant variables (p-value < α), which is in agreement with previous OLS models. More importantly, the plots of residuals against fitted values from both models still suffer from some heteroscedasticity, although reduced (Figure 11). As a result, to overcome the problem of the i.i.d. error

assumption, instead of fitting least square models, this study has employed another type of robust regression, least absolute deviation (LAD).

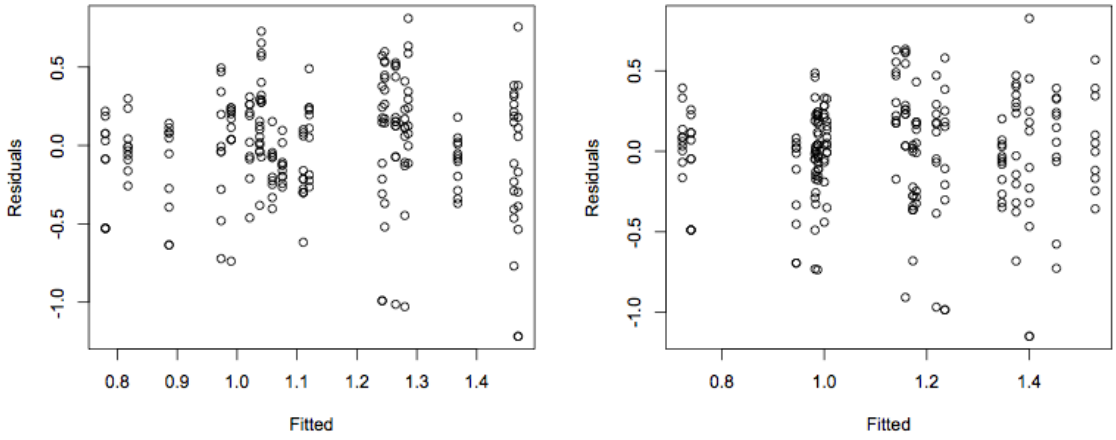

Figure 11. Residuals plotted against fitted value for ordinary least square model 3 (left panel, with Box-Cox transformation) and 4 (right panel, with Box-Cox transformation and polynomials).

The goal of least absolute deviation (LAD) is to estimate $\hat{\beta}$ by minimizing the $\min_{\beta} \sum_{i=1}^{n} |\varepsilon_i| = |y - X\beta|$, instead of minimizing $\min_{\beta} \sum_{i=1}^{n} \varepsilon_i^2 = \varepsilon^T \varepsilon = (y - X\beta)^T (y - X\beta)$. Table 2 lists estimates and confidence intervals of the coefficients from the LAD model. The confidence interval (CI) is used to indicate the reliability of a coefficient estimate instead of only using one single value (also listed in the table). The width of confidence interval (CI) is based on the level of confidence (1-α) and the CI will be widened with higher confidence level. One intuitive way to understand the importance of confidence intervals is that if the origin (0) is included in the CI, it implies that, at the confidence level of 1-α,

the particular variable is considered to be statistically insignificant. In this study, as mentioned above, α (the type I error) is set to be 0.05 and thus the confidence level is 95%. As shown in the results, the OPD is positively correlated with "*time"*, "*number of burrows"* and "*iron addition"*; more importantly, at the confidence level of 95%, "*time"*, "*number of burrows"* and "*iron addition"* are significant variables and should be included in our model.

The results from the statistical analyses conducted above demonstrate the significance of "*time"*, "*number of burrows"* and "*iron addition"* in our model, and thus suggest a critical role of iron in controlling the *oxygen penetration depth (OPD)*. However, since manual oxygen microelectrode measurement is very time consuming, we have only obtained a finite number of measurements (211 profiles for 5 cores) during a limited period of time. Other potential variance may also exist that our data and regression model is not yet able to detect. Thus, we do not expect our model to be extremely thorough and powerful as a general predictor for the marine sediments from Cape Lookout Bight. However, the statistical analyses do guide us to perform one more additional assessment of the data that is quite revealing, discussed further below (Figure 13).

Discussion and Conclusion

This study has developed a new methodology for assessing the biogeochemical role of iron as a sulfide buffer during early diagenesis. Our initial motivation was to test the "Sulfide Buffer/Phosphorous Trap Hypothesis" with modern sediments from Cape Lookout Bight, a sedimentary environment that is dominated by sulfate reduction and methanogenesis. The macrocosm "iron addition" experiments combine both oxygen microelectrode contour mapping and X-ray fluorescence Sm-tracer scanning, which provides "snapshots" of the biogeochemistry in the sediments through time. The results from microelectrode measurements and XRF scans, which exhibit similar magnitude, compare very well. This suggests that our methodology can evaluate marine biogeochemistry from two perspectives, and that oxygen penetration depth (OPD) and bioturbation (Sm ERD) are closely coupled (Figure 12).

In this study we explicitly evaluated the relationship between the reactive iron concentration within surficial sediments and bioturbation/bioirrigation. The oxygen microelectrode analyses enabled us to monitor oxygen penetration into the sediment influenced by bioirrigation, and the samarium tracer allowed us to detect and quantify bioturbation. Both of these factors are related to aerobic organic matter remineralization, and thus can impact organic matter burial (Hartnett et. al, 1998).

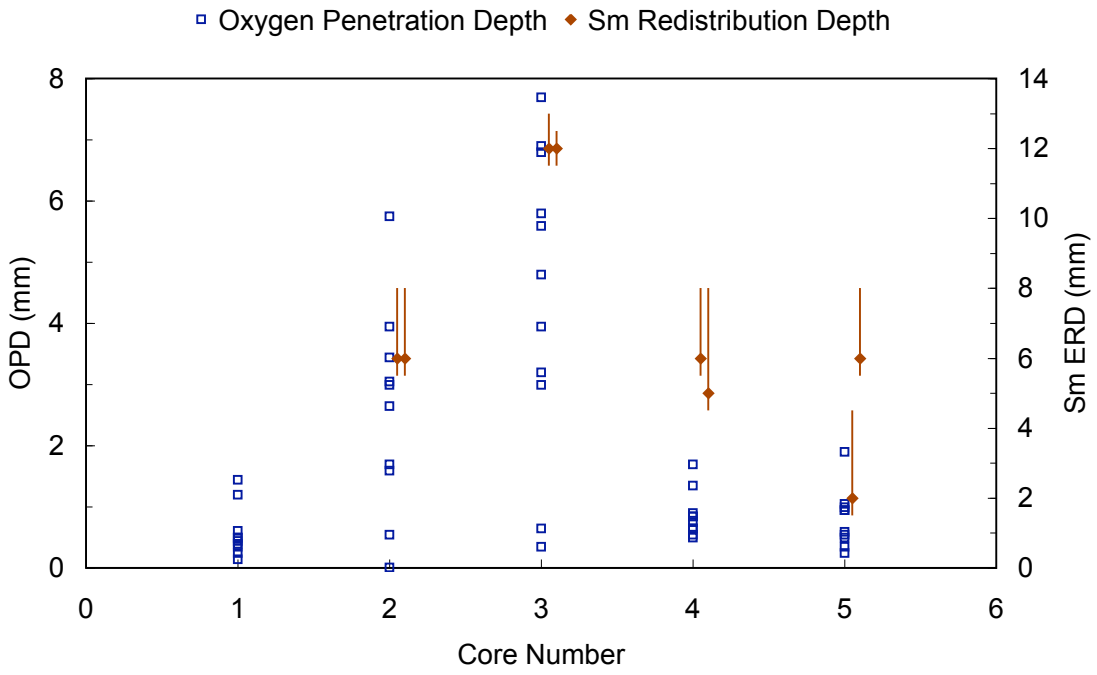

Figure 12. Summary of bioturbation and bioirrigation in the macrocosm experiments. Empty squares (blue) represent OPD during the fourth measurement period, and solid diamonds (red, with 1 s.d.) represent Sm-tracer vertical ERD at the final stage of the experiment. The Sm ERD (bioturbation) matches the trends of OPD, suggesting that the methodology developed in this study has great potential in the study of early diagenesis in marine sediments.

The results from our 3-month "iron addition" experiments indicate that the OPD and the Sm ERD are corroborative, which confirms the robustness of our methodology (Figure 12). The OPD measurements were contoured for initial graphic comparison among different cores (spatial) and measurement periods (temporal). The comparison of temporal patterns from cores 2 and 3 suggest that additional iron input could buffer the accumulation of hydrogen sulfide (H_2S), removing this toxic constituent from the pore

water, and consequently enhancing the degree of bioturbation/bioirrigation by aerobic metazoa. The consequence of this is a deepened oxygen penetration and Sm redistribution (bioturbation). On the contrary, observations from cores 3, 4 and 5 suggest that the number and type of metazoa are also possible constraints on the OPD. Meanwhile, generally deeper OPDs from cores 4 and 5, compared to core 1, also suggest an important role of iron as a buffer for hydrogen sulfide during early diagenesis.

In order to provide a more objective analysis of this experimental data, we employed various regression models to evaluate the relationship between the dependent variable *OPD* and independent variables, such as "*time"*, "*number of burrows"*, "*burrow/nonburrow"* and "*iron addition"*. We discovered that Ordinary Least Squares (OLS) regression is not applicable in this study, because the heteroscedasticity observed in the residual plot indicates that the errors are not independent, and identically distributed (i.i.d.). To address this issue, a Box-Cox transformation was applied on OPD and a Least Absolute Deviation (LAD) model was fitted to explain the variance in OPD. These models emphasize the significance of "*time"*, "*number of burrows"* and "*iron addition"* for the model at the confidence level of 95%, meaning that the variance in OPD could be explained mostly by "*time"*, "*number of burrows"* and "*iron addition"*.

In one final analysis, we now separate out the number of burrows from the pool of significant variables. The data is divided into 3 groups: sparse (0-2 burrows), intermediate (3-5 burrows) and dense (6-8 burrows). Each group has a certain range of burrow numbers, which we take to represent the biological activity level of aerobic

metazoa (e.g., number and type of burrowing organisms). Figure 13 illustrates both the scatter plots and box plots of the relationship between OPD and the amount of iron addition, given the specific range of burrow numbers. That is, the relationship between OPD and iron input is now compared based on similar aerobic biological activity, instead of solely based on time.

We observe that the oxygen penetration depth deepens with increased iron delivery to the sediments within each set burrow number range. In other words, given a similar range of organisms, or, similar aerobic biologic activity level, increased iron input can indeed enhance the degree of bioturbation/bioirrigation by buffering hydrogen sulfide accumulation in the pore water. The results suggest that iron has an important role in early diagenetic processes within sediments, as predicted by the "Sulfide Buffer/Phosphorous Trap Hypothesis".

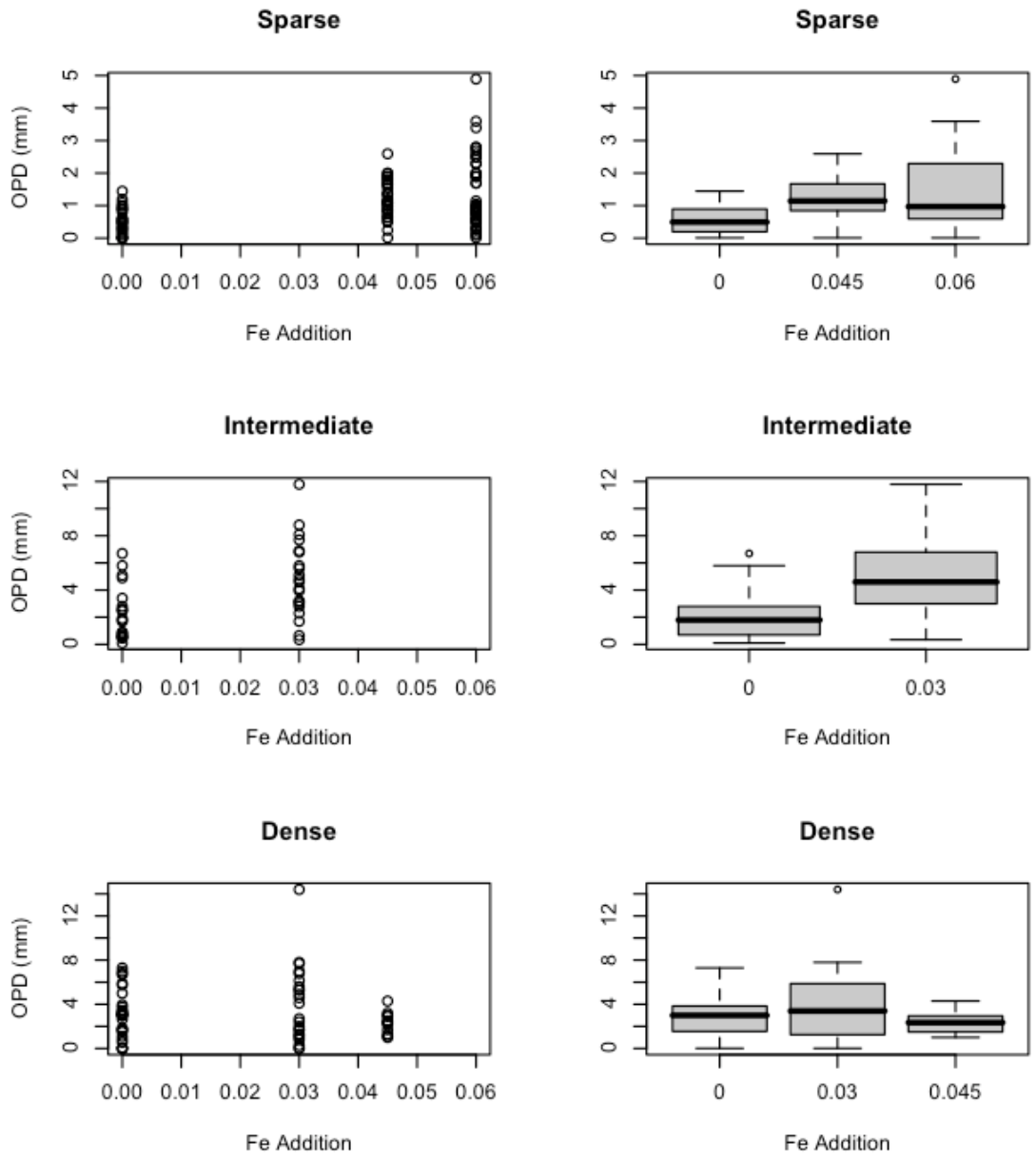

Figure 13. Correlation between the OPD and the amount of iron addition, given different burrow numbers: sparse (0-2), intermediate (3-5) and dense (6-8). The number of the burrows is taken as proxy for the number of bioturbating organisms (degree of macrofaunal activity) in each core. Circles in the scatter plots (left panel) represent OPDs, while box plots (right panel) bracket highest and lowest datum still within 1.5 IQR (interquartile range), with outliers (extreme values) identified in circles.

Future Improvements

The initial focus for our study is the biogeochemical role of iron as a pore water sulfide buffer during early diagenesis. Limited by a finite number of observations, we have not been able to exclude the possibility that other variables may also be important in our incubation experiments. To better understand the significance of iron, it is necessary to rule out iron-unrelated variables like the number of macrofauna as much as possible, given the fact that it still remains very challenging to constrain and quantify biologic activities after the fact, solely based on the descriptors and observations. For future investigation, it is critical to ensure that all the sediment cores share almost identical number and type of metazoa. One possibility is to start with complete sulfidization, by preventing oxygen exchange with the atmosphere (e.g., sealing the core top). The hydrogen sulfide accumulation will eventually shoal the SRZ, and exclude all aerobic biologic activities from the sediments. Identical number and type of aerobic metazoa, collected from the local ecosystem, could then be introduced with the synthetic sediments (consisting of a Sm-tracer element, various amounts of iron addition and clay as the carrier). Moreover, the form of iron can also provide additional information; hematite is selected for this study primarily based on its accessibility and moderate reactivity (similar to the organic matter reactivity in Cape Lookout Bight sediments; Chanton, 1985). Since iron has many forms other than hematite, it would be insightful to include iron reactivity in our model by incorporating other forms of iron as the H_2S buffering agent. These improvements would better constrain the initial conditions of our study and lead to more rigid and detailed regression models.

In addition, the “Phosphorous Trap” aspect of the hypothesis was not addressed in this study. The return flux of phosphate from the sediments, including regenerated phosphorus from organic matter decay and released iron bound phosphorus, is almost one magnitude larger than the riverine input flux globally (Colman and Holland, 2000), and this phosphate return flux is highly redox sensitive (Colman and Holland, 2000). The coupled relationships among iron delivery, phosphate return flux, and redox boundary oscillation within sediments has a very significant potential for controlling organic matter burial, and could have impacted climate change and atmospheric carbon dioxide and oxygen levels (Martin, 1990). Given that iron input, together with phosphorus and some other trace metals, is believed to limit, or at least co-limit primary production in most coastal marine settings (Colman et al., 2005), the next phase of incubation experiment studies should investigate the relationship between phosphorous flux and iron delivery, and further evaluate organic matter burial feedbacks with the global phosphorus cycle. Future studies could also automate the oxygen microelectrode mapping and this would substantially improve the spatial density of OPD measurements and could considerably refine the regression models.

Potential Implication

The results from studies such as that pursued here can provide the basis for the development of quantitative diagenetic models. One of the potential applications of such diagenetic models is to address the causes of ancient organic matter burial events, such as the Cretaceous Oceanic Anoxic Events (e.g., OAE II).

The accumulation of skeletal material (mostly calcite and silicate materials) in marine sediments has a tremendous capacity to regulate reactive iron concentration. Consequently, evolutionary changes in pelagic biomineralization during the Phanerozoic may have played an important role in setting the stage for organic carbon burial events (Meyers, 2007). Previous studies have documented a major evolution of foraminifera and nannofossils during the early Cretaceous. Since foraminifera and nannofossils build their shells mainly out of calcite ($CaCO_3$), this event resulted in the contribution of large amounts of $CaCO_3$ into the sediments, diluting the concentration of iron. Diluted iron concentration could faciliate H_2S accumulation in the sediments, and diminish bioturbation/bioirrigation, resulting in large amounts of organic matter being preserved (Figure 14). Importantly, this time of foraminifera and nannofossil evolution is also associated with major organic matter burial events, known as Oceanic Anoxic Events.

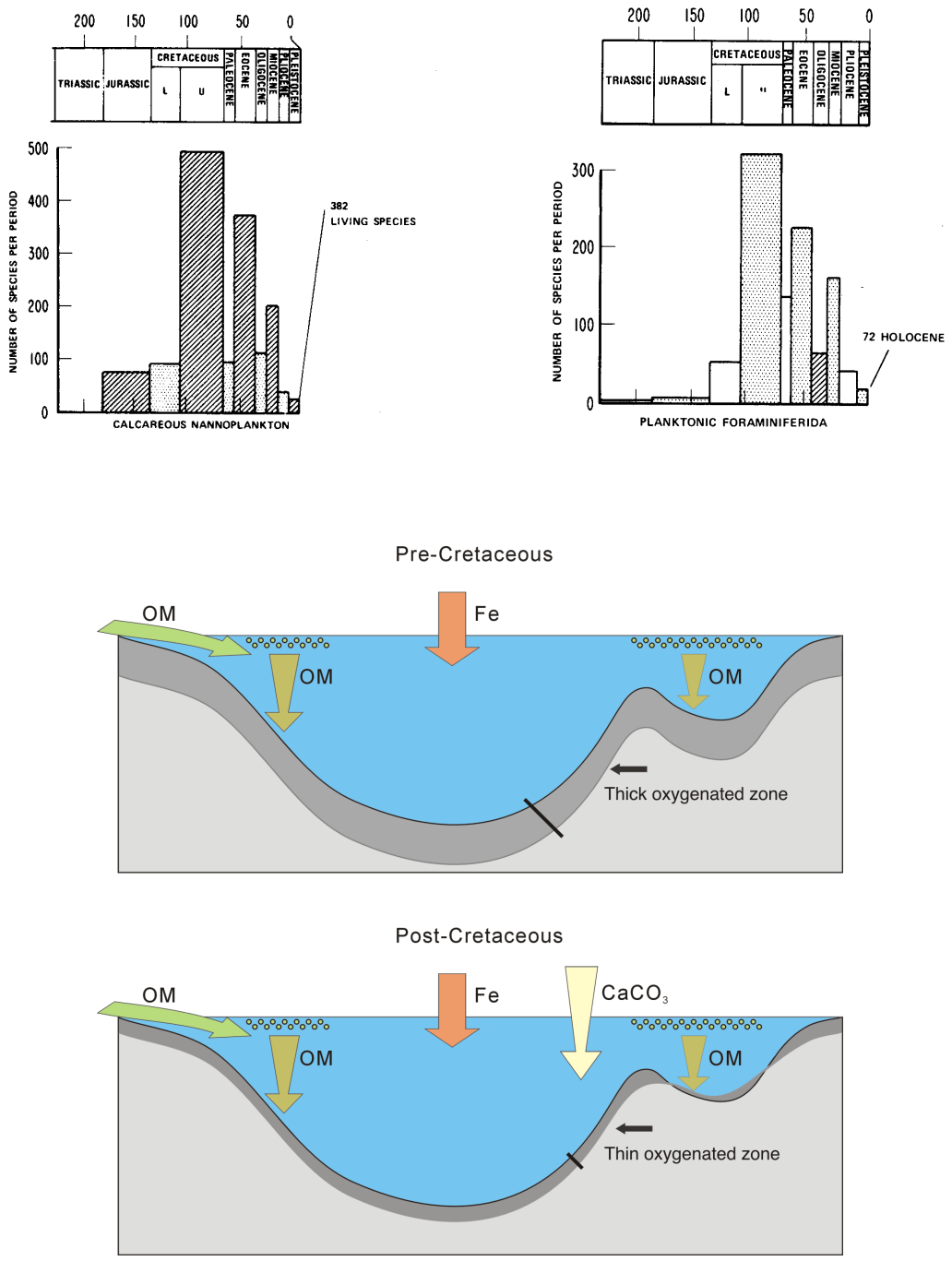

Figure 14. Foraminifera and nannofossil evolution could contribute large amounts of $CaCO_3$, which would have diluted the iron concentration and caused H_2S to accumulate in the sediments during the Cretaceous. (Foraminifera and nannofossils evolution figures from Tappan and Loeblich, 1973)

References

Anderson, T. F., and R. Raiswell (2004), Sources and mechanisms for the enrichment of highly reactive iron in euxinic Black Sea sediments, Am. J. Sci., 304, 203–233.

Canfield, D. E. (1989a), Reactive iron in marine sediments, Geochim. Cosmochim. Acta, 53, 619 – 632.

Canfield, D. E. (1989b), Sulfate reduction and oxic respiration in marine sediments: Implications for organic carbon preservation in euxinic sediments, Deep Sea Res., Part A, 36, 121 – 138.

Chanton, J.P. (1985), Sulfur mass balance and isotopic fractionation in an anoxic marine sediment, Ph.D. thesis, University of North Carolina at Chapel Hill, 406 pp.

Coale, K. H., et al. (1996), A massive phytoplankton bloom induced by an ecosystem-scale iron fertilization experiment in the equatorial Pacific Ocean, Nature, Vol. 383, p.495-501

Colman, A. S. and Holland, H. D. (2000), The global diagenetic flux of phosphorus from marine sediments to the oceans: redox sensitivity and the control of atmosphere oxygen levels: SEPM Special Publication No. 66, p. 53-75

Colman, A. S., et al. (2005), Marine phosphate oxygen isotopes and organic matter remineralization in the oceans, PNAS.0506455102, doi 10.1073

Demaison, G. J. and Moore, G. T. (1980), Anoxic environment and oil source bed genesis: AAPG Bull., v. 64, p. 1179-1209.

Deuser, W. G. (1971), Organic-carbon budget of the Black Sea: Deep-Sea Research, v. 18, p. 995-1004

Grunau, H. R. (1983), Abundance of source rocks for oil and gas worldwide: Journal of Petroleum Geology, v. 6, p. 39-54.

Haddad, R. I., and Martens C. S. (1987) Biogeochemical cycling in an organic-rich coastal marine basin: sources and accumulation rates of vascular plant-derived organic material: Geochimica et Cosmochimica Acta, 51 2991-3001.

Hartnett, H. E. et al. (1998), Influence of oxygen exposure time on organic carbon preservation in continental margin sediments: Nature, v. 391, p. 572-574.

Hedges, J. I. and Keil R. G. (1995), Sedimentary organic matter preservation: an assessment and speculative synthesis: Marine Chemistry, 49, p. 81-115.

Ibach, L. E. J. (1982), Relationship between sedimentation rate and total organic carbon content in ancient marine sediments: AAPG Bull., v. 66, 170-188.

Leckie, R. M. (1985), Foraminifera of the Cenomanian-Turonian boundary interval, Greenhorn Formation, Rock Canyon Anticline, Pueblo, Colorado, in Fine-Grained Deposits and Biofacies of the Cretaceous Western Interior Seaway: Evidence of Cyclic Sedimentary Processes, edited by L. M. Pratt et al., pp. 139 – 149, Soc. for Sediment. Geol., Tulsa, Okla.

Leckie, R. M., T. J. Bralower, and R. Cashman (2002), Oceanic anoxic events and plankton evolution: Biotic response to tectonic forcing during the mid-Cretaceous, Paleoceanography, 17(3), 1041, doi:10.1029/2001PA000623.

Libes, S. (2005), An introduction to marine biogeochemistry, Elsevier, New York.

Martin, J. H. (1990), Glacial-interglacial CO_2 change: The iron hypothesis, Paleoceanography, 5, 1– 13.

Martin, J. H., and S. E. Fitzwater (1988), Iron deficiency limits phytoplankton growth in the north-east Pacific subarctic, Nature, 331, 341–343.

Martin, J. H., R. M. Gordon, S. Fitzwater, and W. W. Broenkow (1989), VERTEX: Phytoplankton/iron studies in the Gulf of Alaska, Deep Sea Res., Part A, 36, 649–680.

Martin, J. H., et al. (1994), Testing the iron hypothesis in ecosystems of the equatorial Pacific Ocean, Nature, 371, 123–129.

Meyers, S. (2007), Production and preservation of organic matter: The significance of iron: Paleoceanography, v. 22, PA4211, doi:10.1029/2006PA001332.

Meyers, S. R., B. B. Sageman, and T. W. Lyons (2005), Organic carbon burial rate and the molybdenum proxy: Theoretical framework and application to Cenomanian-Turonian oceanic anoxic event 2, Paleoceanography, 20, PA2002, doi:10.1029/2004PA001068.

Meyers, P. A. (2006), Paleoceanographic and paleoclimatic similarities between Mediterranean sapropels and Cretaceous black shales, Palaeogeorg. Palaeoclimatol. Palaeoecol., 235, 305–320.

Meyers, S. R. (2003), Integrated cyclostratigraphy and biogeochemistry of the Cenomanian/Turonian boundary interval, Western Interior Basin, North America, 393 pp., Ph.D. thesis, Northwestern Univ., Evanston, Ill.

Meyers, S. R., and B. B. Sageman (2004), Detection, quantification, and significance of hiatuses in pelagic and hemipelagic strata, Earth Planet. Sci. Lett., 224, 55–72.

Meyers, S. R., B. B. Sageman, and L. A. Hinnov (2001), Integrated quantitative stratigraphy of the Cenomanian-Turonian Bridge Creek Limestone Member using evolutive harmonic analysis and stratigraphic modeling, J. Sediment. Res., 71, 627– 643.

Perdersen T. F. and Calvert S. E. (1990), Anoxia vs. productivity: What controls the formation of organic-carbon-rich sediments and sedimentary rocks: AAPG Bull., v. 74, p. 454-466.

Prufert, L. (1985), Seasonal variations of iron and manganese diagenesis in an organic rich coastal marine basin. M.S. thesis, University of North Carolina at Chapel Hill.

Ruttenberg, K. C. (2003), The global phosphorous cycle, in Treatise on Geochemistry, vol. 8, edited by W. H. Schlesinger, pp. 585–643, Elsevier, New York.

Sageman, B. B., A. E. Murphy, J. P.Werne, C. A. Ver Straeten, D. J. Hollander, and T. W. Lyons (2003), A tale of shales: The relative roles of production, decomposition, and

dilution in the accumulation of organic-rich strata, Middle-Upper Devonian, Appalachian basin, Chem. Geol., 195, 229–273.

Sageman, B. B., and T. Lyons (2004), Geochemistry of fine-grained sediments and sedimentary rocks, in Treatise on Geochemistry, vol. 7, edited by F. MacKenzie, pp. 115–158, Elsevier, New York.

Tappan, H., and A. R. Loeblich (1973), Evolution of the ocean plankton, Earth Sci. Rev., 9, 207–240.

Toth, D. J., and A. Lerman (1977), Organic matter reactivity and sedimentation rates in the ocean, Am. J. Sci., 277, 465– 485.

Table 1. Procedures for incubation experiments

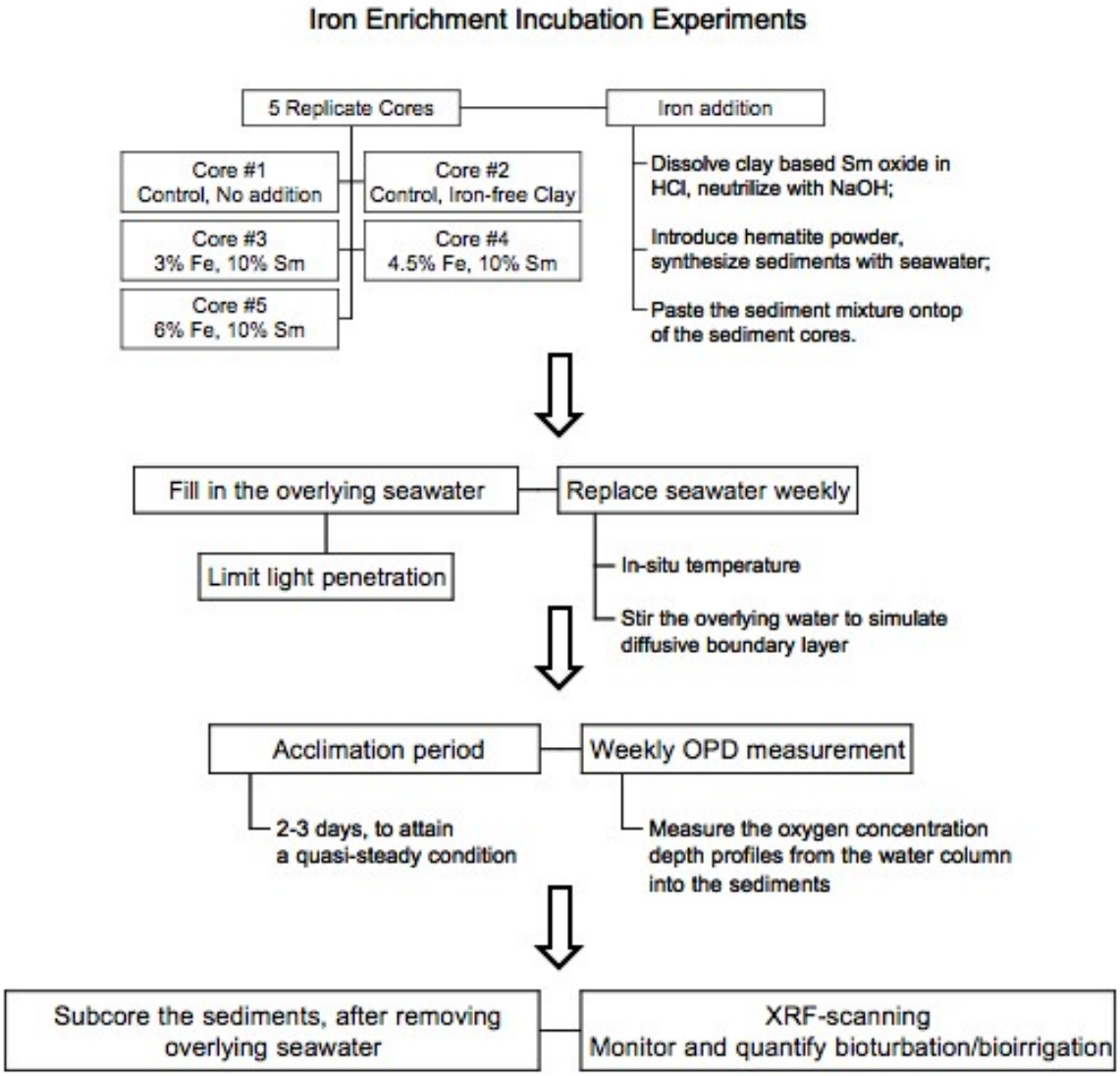

Table 2. Statistical regression results

Ordinary Least Square (OLS-1)

Call:
lm(formula = OPD ~ Time + BurrowNbr + Burrow + Fe, data = dat)

Coefficients:					
	Estimate	Std. Error	t value	Pr(>|t|)	
(Intercept)	0.040469	0.424832	0.095	0.924	
Time	0.006489	0.00399	1.627	0.105	
BurrowNbr	0.445225	0.064204	6.934	5.16E-11	***
Burrow	0.036306	0.351922	0.103	0.918	
Fe	14.689621	6.31624	2.326	0.021	*

Signif. codes: 0 '***' 0.001 '**' 0.01 '*' 0.05 '.' 0.1 ' ' 1

Residual standard error: 2 on 206 degrees of freedom
Multiple R-squared: 0.2453, Adjusted R-squared: 0.2307
F-statistic: 16.74 on 4 and 206 DF, p-value: 6.735e-12

Ordinary Least Square (OLS-2)

Call:
lm(formula = OPD ~ Time + BurrowNbr + Fe, data = dat)

Coefficients:					
	Estimate	Std. Error	t value	Pr(>|t|)	
(Intercept)	0.04088	0.423796	0.096	0.9232	
Time	0.006501	0.003978	1.634	0.1038	
BurrowNbr	0.448377	0.056334	7.959	1.12E-13	***
Fe	14.673646	6.299234	2.329	0.0208	*

Signif. codes: 0 '***' 0.001 '**' 0.01 '*' 0.05 '.' 0.1 ' ' 1

Residual standard error: 1.995 on 207 degrees of freedom
Multiple R-squared: 0.2453, Adjusted R-squared: 0.2344
F-statistic: 22.43 on 3 and 207 DF, p-value: 1.296e-12

Table 2 continued

Ordinary Least Square after transformation on response (OLS-3)

Call:
lm(formula = I(OPD^0.3) ~ Time + BurrowNbr + Fe, data = dat)

Coefficients:					
	Estimate	Std. Error	t value	Pr(>|t|)	
(Intercept)	0.7183437	0.0756831	9.491	< 2E-16	***
Time	0.0009937	0.0007105	1.399	0.163425	
BurrowNbr	0.0770383	0.0100602	7.658	7.13E-13	***
Fe	4.0166516	1.1249399	3.571	0.000443	***

Signif. codes: 0 '***' 0.001 '**' 0.01 '*' 0.05 '.' 0.1 ' ' 1

Residual standard error: 0.3563 on 207 degrees of freedom
Multiple R-squared: 0.2324, Adjusted R-squared: 0.2213
F-statistic: 20.89 on 3 and 207 DF, p-value: 7.298e-12

Ordinary Least Square after transformation on response and Polynomial (OLS-4)

Call:
lm(formula = I(OPD^0.3) ~ poly(Time, 3)+poly(BurrowNbr, 3)+poly(Fe, 3), data = dat)

Coefficients:					
	Estimate	Std. Error	t value	Pr(>|t|)	
(Intercept)	1.13632	0.024	47.353	< 2E-16	***
poly(Time, 3)1	0.13786	0.47729	0.289	0.773002	
poly(Time, 3)2	-0.16509	0.37756	-0.437	0.662396	
poly(Time, 3)3	0.08783	0.39494	0.222	0.824236	
poly(BurrowNbr, 3)1	2.53578	0.67498	3.757	0.000225	***
poly(BurrowNbr, 3)2	-1.25893	0.37044	-3.398	0.000817	***
poly(BurrowNbr, 3)3	-0.34632	0.46745	-0.741	0.459631	
poly(Fe, 3)1	1.47445	0.42313	3.485	0.000605	***
poly(Fe, 3)2	-0.75415	0.54991	-1.371	0.171778	
poly(Fe, 3)3	0.88525	0.3987	2.22	0.027512	*

Signif. codes: 0 '***' 0.001 '**' 0.01 '*' 0.05 '.' 0.1 ' ' 1

Residual standard error: 0.3486 on 201 degrees of freedom
Multiple R-squared: 0.2866, Adjusted R-squared: 0.2547
F-statistic: 8.973 on 9 and 201 DF, p-value: 2.362e-11

Table 2 continued

Robust regression
Least Absolute Deviation

Call: rq(formula = OPD ~ Time + BurrowNbr + Fe)

tau: [1] 0.5

Coefficients:			
	coefficients	lower bd	upper bd
(Intercept)	0.14561	-0.0827	0.45474
Time	0.00291	0.0003	0.00536
BurrowNbr	0.40407	0.33686	0.4504
Fe	11.20155	7.74799	14.0082

Appendix A. Locating the sediment-water interface in O_2 microsensor profiles (These methods are provided by Marc Alperin)

Constraints

1. *Bottom-up approach*. Oxygen concentrations in fine-grained sediments are described by the following equation:

$$\frac{d}{dx}\left(\varphi D_s \frac{dc}{dx}\right) - \varphi R = 0$$

$$D_s = \varphi^2 D_o$$

$$\therefore \varphi^2 D_o \frac{d^2c}{dx^2} + 3\varphi D_o \frac{d\varphi}{dx}\frac{dc}{dx} - R = 0$$

$$\text{and } \varphi^2 D_o \frac{d^2c}{dx^2} = R - 3\varphi D_o \frac{d\varphi}{dx}\frac{dc}{dx}$$

where c is oxygen concentration, x is depth below the sediment-water interface, φ is porosity, D_o and D_s are the molecular and sediment diffusivity for oxygen, respectively, and R is the oxygen consumption rate. Oxygen profiles within the sediment should be concave up ($d^2c/dx^2 > 0$) provided that:

   a. There is no photosynthetic oxygen production (a reasonable assumption provided the sediments are kept in the dark);

   b. The oxygen profile is at steady-state (the time to steady-state is on the order of the 5-20 minute [$L^2/2D_s$, where L is the oxygen penetration depth (1-2 mm) and D_s is the molecular diffusivity for oxygen]);

   c. Advection can be neglected (this assumption is supported by the Peclet number [wL/D_s] Pe ~ 10^{-4}),

d. $R > 3\varphi D\ d\varphi/dx\ dc/dx$ (although this is probably true for most estuarine sediments where R is large and $d\varphi/dx$ is small, it warrants a closer look),

e. Surface topography is uniformly flat,

f. Bioirrigation is not important.

There might be a sudden change in concavity at the sediment-water interface due to the rapid transition from D_s to D_o (i.e., large $d\varphi/dx$) if surface sediments have moderate to low porosity (<0.8). (Note that D_s differs from D_o by < 10% if $\varphi_o >$ 0.95.)

To constrain the sediment-water interface, begin below the oxygen penetration depth and look for the first horizon where the oxygen profile is no longer concave up. In the best cases, the horizon where the profile approaches linearity from below will occur at a depth where the slope suddenly becomes less negative.

Sand layers or other discontinuities in lithology can generate kinks in the oxygen profile within the sediment. These 'kinks' should be ignored if they imply an oxygen penetration depth or diffusive boundary layer thickness that is well-outside the expected range.

2. *Top-down approach*. Oxygen profiles within some portion of the diffusive boundary layer should be linear provided that:

   a. Turbulent diffusion << molecular diffusion;

   b. Oxygen consumption or production is not occurring within the water column.

To constrain the sediment-water interface, begin above the diffusive boundary layer, look for the region where the oxygen profile first becomes linear, and draw a line that best-fits the linear portion of the profile. The sediment-water interface is identified as the lower horizon where oxygen concentrations deviate from the line. In the best cases, oxygen concentrations just below the sediment-water interface will lie above the line that is extrapolated from the linear portion of the profile.

3. *Locate 'kink'*. The flux must be continuous at the sediment-water interface. Therefore, the flux from above and below must be equal.

$$F_+ = -D\left(\frac{dc}{dx}\right)_+ = F_- = -\varphi D_S\left(\frac{dc}{dx}\right)_- \cong -\varphi^3 D\left(\frac{dc}{dx}\right)_- .$$

$$\therefore \left(\frac{dc}{dx}\right)_+ = \varphi^3\left(\frac{dc}{dx}\right)_- .$$

To maintain continuity at the sediment surface, the gradient must change by a factor of φ^3. If interface porosity is 0.9, slope should change by >25%. However, the 'kink' is often not apparent in the profiles. This may be due to the presence of a floc layer, three-dimensional topography, and/or limited resolution of the microelectrode.

4. *Down/Linear/Up*. The oxygen profile should be concave-down through the transition layer, linear through the diffusive boundary layer, and concave-up below the sediment-water interface. (This is not exactly true in that the large negative porosity gradient at the sediment-water interface can induce downward concavity just below the sediment surface.) The sediment surface should be

located at or just above the transition from linear to concave-up. This point can be used for the *flux balance* check described below.

5. *Flux constraint*. The constraint that $F_+ = F_-$ can aid in locating the sediment-water interface. F_+ can be evaluated by linear regression of O_2 vs. depth data from the linear portion of the profile below the transition layer and above the sediment-water interface. Uncertainty in F_+ can be estimated from uncertainty in the slope of the linear regression. The value of F_+ is not very sensitive to the exact location of the sediment-water interface. F_- can be estimated by integrating the reaction rate depth distribution estimated by inverse modeling the oxygen profile. The integrated rate is sensitive to the location of the sediment-water interface. If F_- is inconsistent with F_+ suggests that the presumed location of the sediment surface is incorrect.

   Notes on determining rates from inverse modeling:

   a. Set relative error for first 2 points to zero (0.001%) to assure that flux is accurate.

   b. Set relative error to 10% for O_2 concentrations $\leq$1 mM.

   c. Vary relative error (one value for all other points) to reduce high frequency oscillations in second derivative.

6. *Variance approach*. Turbulent eddy penetration is inhibited in the vicinity of the sediment-water interface. It may be possible to constrain the location of the sediment-water interface by examining temporal fluctuations in oxygen

concentrations at each horizon over time. As Gunderson and Jorgensen point out, "the transition from stable to fluctuating oxygen concentration is not a reproducible indicator of the sediment-water interface because the position of the transition varies with flow velocity." However, the turbulent fluctuations could provide an independent check on the location of the sediment-water interface constrained by the "bottom-up" and "top-down" approaches. We need more experience with oxygen time-series to evaluate whether this will pan out.

7. *DBL constraint*. Published values for the thickness of the diffusive boundary layer range from 0.2 to 1 mm (in situ and stirred chambers). The top of the diffusive boundary can usually be determined as the point where oxygen concentrations first begin to drop below bottom-water values. If the presumed sediment surface is <<0.2 mm or >>1 mm below the top of the DBL, the presumed location of the interface is likely to be in error.

8. *Direct measurement*. Roy et al. describe a laser-digital camera system for mapping the sediment surface. Optical fibers inserted into the sediment from below and aligned precisely with the sediment-water interface were used to determine the location of the microsensors relative to the sediment-water interface.

Tips for microelectrode profiling

1. Make at least 4 measurements above the diffusive boundary layer (necessary for defining the top of the DBL).

2. Use maximum resolution in the DBL (necessary for defining the linear region and providing a strong constraint on flux).

3. If oxygen values in the DBL appear to be noisy or erratic, abandon the profile and start over again (noisy data in the DBL make it difficult to establish the flux constraint).